Inorganic Hollow Nanotube Aerogels by Atomic Layer Deposition onto Native Nanocellulose Templates

Juuso T. Korhonen,[†] Panu Hiekkataipale,[†] Jari Malm,[‡] Maarit Karppinen,[‡] Olli Ikkala,[†] and Robin H. A. Ras[†,*]

[†]Molecular Materials, Department of Applied Physics, Aalto University (formerly Helsinki University of Technology), Puumiehenkuja 2, 02150 Espoo, Finland and [‡]Laboratory of Inorganic Chemistry, Aalto University, Kemistintie 1, 02150 Espoo, Finland

ABSTRACT Hollow nano-objects have raised interest in applications such as sensing, encapsulation, and drug-release. Here we report on a new class of porous materials, namely inorganic nanotube aerogels that, unlike other aerogels, have a framework consisting of inorganic hollow nanotubes. First we show a preparation method for titanium dioxide, zinc oxide, and aluminum oxide nanotube aerogels based on atomic layer deposition (ALD) on biological nanofibrillar aerogel templates, that is, nanofibrillated cellulose (NFC), also called microfibrillated cellulose (MFC) or nanocellulose. The aerogel templates are prepared from nanocellulose hydrogels either by freeze-drying in liquid nitrogen or liquid propane or by supercritical drying, and they consist of a highly porous percolating network of cellulose nanofibrils. They can be prepared as films on substrates or as freestanding objects. We show that, in contrast to freeze-drying, supercritical drying produces nanocellulose aerogels without major interfibrillar aggregation even in thick films. Uniform oxide layers are readily deposited by ALD onto the fibrils leading to organic–inorganic core–shell nanofibers. We further demonstrate that calcination at 450 °C removes the organic core leading to purely inorganic self-supporting aerogels consisting of hollow nanotubular networks. They can also be dispersed by grinding, for example, in ethanol to create a slurry of inorganic hollow nanotubes, which in turn can be deposited to form a porous film. Finally we demonstrate the use of a titanium dioxide nanotube network as a resistive humidity sensor with a fast response.

KEYWORDS: microfibrillated cellulose (MFC) · nanofibrillated cellulose (NFC) · chemical vapor deposition (CVD) · nonwoven fiber · nanofiber

One-dimensional nanostructures with lateral dimensions below 100 nm, including nanowires and nanotubes, are a technologically important class of materials with unique thermal, electronic, optical, and mechanical properties, and they are feasible in applications as nanoscale building blocks for functional materials and devices.[1] Inorganic nanowires, for example, have spurred research toward single-molecule detection, energy harvesting, nanoelectromechanical systems, and detection of neural signals.[2] Inorganic nanotubes have been pursued in optoelectronics, sensors, drug release, and fluid manipulation.[3] During recent years, many routes toward hollow inorganic nano-objects have been demonstrated, including templating on nanoporous membranes or nanofibers, for example, coating anodic alumina membranes by various methods,[4–8] directly anodizing titanium dioxide films,[9] coating electrospun fibers,[10,11] and coating block copolymer templates with inorganics.[12] In this context, also aerogels could be particularly useful as facile highly porous network-like solid templates for inorganic nanotubes.

Highly porous solid materials, called aerogels, were first discovered in the 1930s,[13] and although silica aerogels were commercially produced already in the 1940s,[14] it was not until late 20th century when a more broad range of applications was introduced.[15,16] Nowadays several types of aerogels are made by sol–gel chemistry. In addition to silica, aerogels can be made from several different materials, such as polymers (including cellulose), which can then in turn be pyrolyzed to carbon aerogels.[15–21] Also metals and metal oxides, such as aluminum oxide and zinc oxide,[22,23] have been used to form aerogels.

Cellulose is an interesting sustainable and natural polymer. Native cellulose forms a hierarchically ordered material, where the individual cellulose polymer chains first crystallize into nanofibrils of *ca.* 3–15 nm diameter, which then pack into larger fibers of several tens of nanometers,[24] and finally into macroscopic fibers of micrometer dimensions. The native nanofibrils can be cleaved by several ways to form nanocellulose hydrogels.[25–29] Usually the material is called nanofibrillated cellulose (NFC) or alternatively microfibrillated cellulose (MFC). While NFC is interesting in itself, it is also attractive as a biological template for functionalities.

Cellulose hydrogels can be dried to form percolating networks, that is, aerogels, and

* Address correspondence to robin.ras@tkk.fi.

Received for review November 8, 2010 and accepted February 14, 2011.

Published online March 01, 2011
10.1021/nn200108s

TABLE 1. Comparison among Different Aerogel Preparation Methods

	method	structure	aggregation	observations
a	freeze-drying by immersion in liquid nitrogen and ice sublimation	aerogel	sheetlike aggregates	
b	freeze-drying by immersion in liquid propane and ice sublimation	aerogel	no aggregation in thin samples	aggregation can occur in thick samples
c	supercritical CO_2 drying from acetone organogel	aerogel	no aggregation	no aggregation even in thick samples
d	drying under ambient conditions	collapsed	sheets parallel to substrate	paper- or plastic-like appearance

they have been prepared from chemically modified,[30] solubilized,[31,32] and native cellulose[33,34] by supercritical drying and freeze-drying. Typically cellulose aerogels have suffered from brittleness, but the native cellulose aerogels have shown attractive mechanical properties, ductility, and flexibility.[33−38] This has encouraged development of aerogels with electrical, optical, and magnetic functionalities.[33,34,39,40]

Atomic layer deposition (ALD) is a sequential, self-limiting chemical vapor deposition method, which enables control of the deposited thickness by the number of cycles instead of the deposition time.[41−44] The gaseous ALD precursors are released into a sample chamber one at a time and then allowed to react with the surface groups of the sample before the reaction byproduct and unreacted precursor molecules are purged from the chamber. The second precursor is then introduced and the cycles are repeated until the desired film thickness is reached. A unique characteristic of ALD is that it forms very uniform films with almost atomic precision on planar substrates but also on complex three-dimensional porous substrates, because the sequential reactions allow long diffusion times for the precursors.[45−51] ALD usually employs lower temperatures than normal chemical vapor deposition. The deposited materials are mostly oxides, but also metals, nitrides, polymers and organic−inorganic hybrid materials have been prepared.[44]

Here we describe a facile method for preparation of hollow inorganic nanotubes by coating nanocellulose aerogels with different oxide materials using ALD, followed by temperature-induced decomposition of cellulose, that is, calcination. As a demonstration for functionality, we show that a film made from TiO_2 nanotubes acts as a resistive humidity sensor with relatively rapid response times.

RESULTS AND DISCUSSION

Comparison of Aerogel Preparation Methods. Nanocellulose hydrogels (see Materials and Methods) can be dried to form aerogels provided that collapse of the fibrillar structure is avoided. Collapse normally occurs during water evaporation because capillary forces pull the fibrils together. Crucial to aerogel preparation is to avoid the direct liquid-to-gas phase transition, by going around the transition line either through liquid-to-solid and solid-to-gas transitions (*i.e.*, freeze-drying) or by going around the critical point of the medium (*i.e.*, supercritical drying).

In this work we made nanocellulose aerogels by three distinct methods: (a) freeze-drying in liquid nitrogen (at boiling point −196 °C) or (b) in cooled liquid propane (boiling point −42 °C, cooled to −100 °C) followed by ice sublimation in vacuum, or (c) supercritical CO_2 drying. For comparison, we made a sample by (d) evaporation of liquid water from nanocellulose hydrogel under ambient conditions. A comparison between the preparation techniques is summarized in Table 1, and scanning electron microscopy (SEM) micrographs of the observed structures along with a summary of the preparation methods are shown in Figure 1 (see Supporting Information Figures S2−S4 for higher resolution micrographs).

Freeze-drying by freezing the nanocellulose hydrogel in liquid nitrogen followed by sublimation of ice in vacuum results in large sheetlike aggregates, which are connected to each other by cellulose fibrils. Large pores can be seen to form on the top of the film. It has been proposed that the sheets and pores result from growing ice crystals pushing the fibrils into sheets, which then meet at the interfaces of the crystals.[35,40] Liquid propane cooled well below the boiling point is more efficient in transferring heat than liquid nitrogen, because it does not boil when the hydrogel is immersed in it. The Leidenfrost effect,[52] that is, the formation of an insulating gas layer, is suppressed, and thus plunging thin hydrogel samples into liquid propane leads to nearly instant freezing. Therefore ice crystals are smaller and the original nanofibrillar network structure is better preserved upon freezing and sublimation of ice. The resulting structure consists mostly of small fibrils with only few fibril aggregates. Note that there are no sheets formed in contrast to the liquid nitrogen freeze-drying, and the structure is similar throughout the film with essentially no aggregation up to about 2 mm thick films. However, increasing the film thickness further will eventually lead to sheetlike aggregation and "cell" formation in the center of the film where the two ice crystal fronts meet (*cf.* Supporting Information Figure S3). Because of different thermal expansion for the substrate and the film, there can be cracks in thick films.[33] Supercritically dried samples are fibrillar throughout over 15 mm thick samples and no clear aggregation to sheets is observed. Also no cracks exist in the monoliths. Although

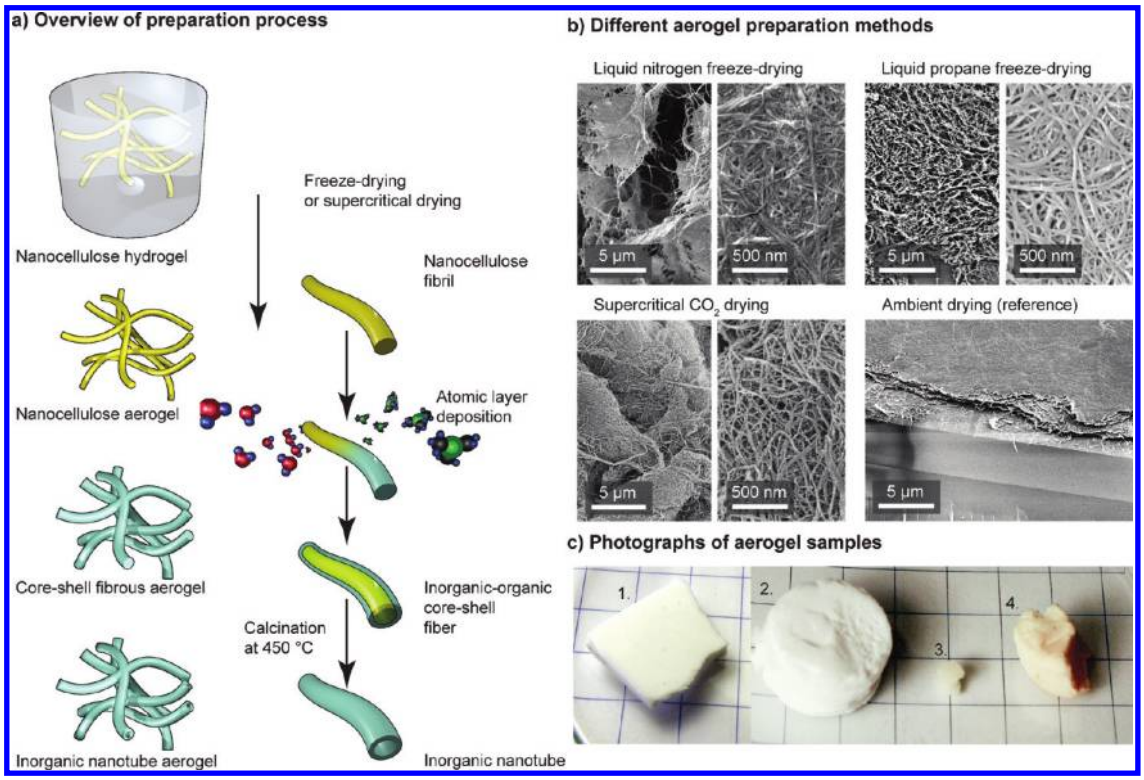

Figure 1. (a) Schematic representation of the preparation processes. First nanocellulose hydrogel is dried to aerogel, which is then coated with inorganic oxides using ALD to form composite organic/inorganic nanofibers, and finally calcinated to inorganic hollow nanotubes. (b) SEM images demonstrating effect of the different drying methods: freeze-drying by freezing nanocellulose hydrogel in liquid nitrogen followed by sublimation of ice in vacuum leads to aerogels with sheetlike aggregates; freeze-drying in liquid propane leads to a fibrillar aerogel with suppressed aggregation, taken the sample is sufficiently thin; supercritical drying leads to fibrillar aerogels essentially without aggregates even in thick samples; drying in ambient conditions leads to collapse of the structure. (c) Photographs of the aerogel samples: (1) Liquid propane freeze-dried aerogel of 2 mm thickness; (2) supercritically dried sample with *ca.* 12 mm diameter and 10 mm height; (3) atmospherically dried sample, which has collapsed completely. Wet dimensions were the same as in the supercritically dried sample; (4) supercritically dried aerogel after ALD shows a slight yellow color on the surface.

the solvent exchange process is slow, supercritical drying is worthwhile if highly fibrillar aerogels without aggregation are wanted. A potential drawback of supercritical drying is that the water in the hydrogel cannot be directly exchanged to CO_2, but instead intermediately has to be exchanged to an organic solvent (here to acetone) to form an organogel. The organic solvent has to be selected such that it mixes well both with water and CO_2 and that it does not significantly modify the network structure of cellulose fibrils. Finally, letting the water freely evaporate from the hydrogel leads to a collapsed thin film of nanocellulose. A close-up reveals some single fibrils, but in general the structure is very dense and consists of sheets mostly parallel to the substrate.

Inorganic–Organic Aerogels by Atomic Layer Deposition onto Nanocellulose Aerogel Templates. Zinc oxide (ZnO), titanium dioxide (TiO_2), and aluminum oxide (Al_2O_3) were deposited on the fibrillar nanocellulose aerogels, and they formed uniform inorganic layers on the fibrils as seen in Figure 2. Even though cellulose aerogels are reported to withstand temperatures up to 275 °C,[36] we observed slight yellow color on the surfaces of the samples after deposition. The growth-per-cycle (GPC) values of the ALD processes were determined from the thicknesses measured using transmission electron microscopy (TEM). The initial layer thickness value is the thickness where the growth saturates when the first pulse of precursor is fed into the sample chamber. The growth of a few nanometer thick inorganic layer on nanocellulose upon a single pulse of titanium isopropoxide was reported recently.[40] Our initial layer thickness was mostly dependent on how well the sample was dried before the deposition process, and all values were 0–3 nm as a result of careful drying. The GPC values were between 0.09 and 0.11 nm for all precursors. To ensure that the initial layer growth was saturated after the first precursor pulse, a sample was further exposed to two subsequent long pulses of the precursor. No differences in the layer thicknesses were observed between these two samples, which in turn supports that the initial layer growth had saturated before the first pulse was over. SEM and TEM images of the coated aerogels show that there were differences between the different oxides. While Al_2O_3 and TiO_2 allowed very uniform and smooth layers, ZnO lead to a more rough coating due to crystallite formation. In all cases, the fibers have not

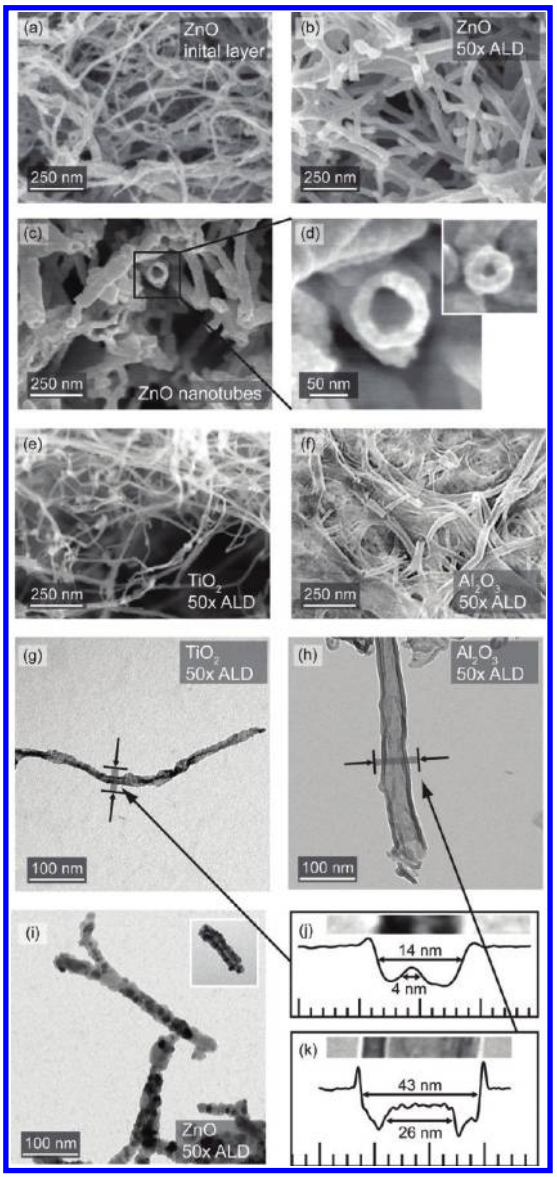

Figure 2. SEM (a-f) and TEM (g-i) of ALD coated aerogels. The number of ALD cycles is indicated in each figure. (a) A thin uniform ZnO layer formed on nanocellulose fibrils after initial exposure to the zinc precursor. (b) ZnO layer thickness is increased upon the ALD process (here 50 cycles). (c) Calcinated, hollow ZnO nanotubes are visibly rough. (d) Close-ups on ZnO nanotubes show that they are hollow. (e) TiO_2 nanotube aerogel. (f) Hollow Al_2O_3 nanotube aerogel. (g) A hollow TiO_2 nanotube, showing some roughness due to crystallization. (h) A hollow Al_2O_3 nanotube demonstrating smooth uniform coating. (i) A hollow ZnO nanotube has undergone crystallization, making the hollow tube interior difficult to resolve. The inset shows a ZnO-coated fibril before calcination. (j) An intensity profile across a hollow TiO_2 nanotube. (k) An intensity profile across a hollow Al_2O_3 nanotube.

fused together to form sheets or other larger aggregates (*cf.* Supporting Information Figure S5), but they represent a coated replica of the original aerogel structure.

Inorganic Hollow Nanotube Aerogels. The cellulose cores of the coated aerogels were easily removed by calcination at 450 °C under air for an extended

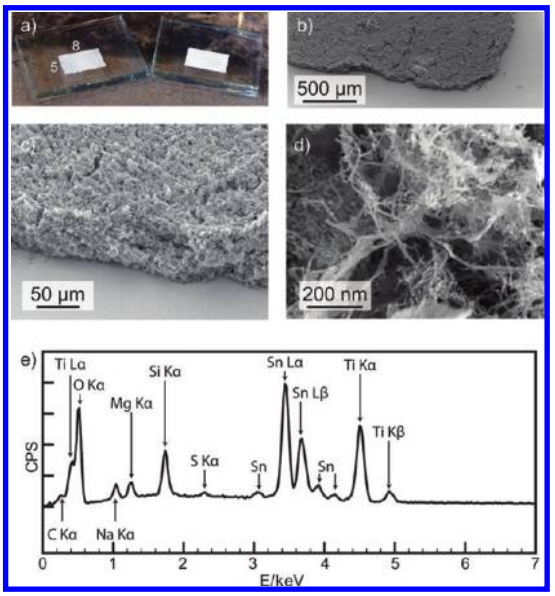

Figure 3. Films cast from a crushed hollow TiO_2 nanotube dispersion in ethanol. (a) Photographs of a 15 (left) and 25 μm (right) thick films. Film dimensions are 5 $\times$ 8 mm. (b) Tilted SEM image shows that the TiO_2 film (*ca.* 50 μm thick) with only a few cracks has formed on the substrate. (c) Larger magnification shows the edge of the film. The film consists of granules of micrometer dimensions. (d) High magnification image shows that the granules are formed of networks of TiO_2 tubes. (e) Energy dispersive X-ray spectrum shows that there is only very little carbon in the film and the TiO_2 content is high. Other peaks originate from the FTO glass.

period of time to form hollow inorganic tubes. The material contracts slightly, which can lead to cracks on the film, but even large samples are still self-supporting, although unlike the pristine nanocellulose and ALD-coated nanocellulose aerogels, they are brittle. SEM reveals the hollow structure (Figure 2), where the inner diameter depends on whether there was an individual cellulose fibril or a bundle of fibrils on the template. Al_2O_3 creates very uniform coatings on the fibrils, which are preserved upon calcination, while the TiO_2-coated fibers crystallize during the calcination. Zinc oxide shows a rough surface already after the ALD process, and it is even more pronounced after calcination. The structure of the aerogel is well preserved after calcination.

Dispersed Nanotubes. The inorganic nanotube aerogels can be crushed in a mortar and dispersed, for example, in ethanol to create a slurry of hollow nanotubes, where the nanotubes form aggregates, which have a porous aerogel-like structure upon solvent evaporation. The size of the aggregates in the slurry can be controlled by sonicating and by mechanical grinding, and from the slurry it is easy to dropcast films of hollow nanotubes onto substrates. We casted TiO_2 nanotube films with thicknesses ranging from 5 to 50 μm on fluorine tin oxide (FTO) coated glass substrates (see Figure 3).

Photographs of dropcast TiO_2 films show that the films have formed smoothly on the substrate and only a small amount of cracking is observed (Figure 3). Higher magnification images show that the aggregates are micrometer sized and they consist of a porous network of TiO_2 nanotubes. Energy dispersive X-ray (EDX) spectrum taken from top of the film shows large titanium and oxygen peaks, while the amount of carbon can be calculated to be less than 1% by weight, which confirms that the organic core has been emptied by thermal decomposition of cellulose into small gaseous molecules such as carbon dioxide and water. The gases can diffuse out from open tube ends, but may also pass through the ALD-grown inorganic coating, similar to what has been observed for ALD-coated polymeric nanorods.[12] The other peaks observed in the EDX spectrum are from either the glass substrate or the FTO layer on the glass. The crystalline structure of the TiO_2 nanotubes was assessed by X-ray diffraction (XRD). From the patterns we identified that there is mostly anatase (see Supporting Information), which is expected after the calcination.

TiO_2 Nanotube Film as a Humidity Sensor. Nanowire sensors have been amply demonstrated based on different semiconducting nanowires between two electrodes.[53−55] It is interesting to explore whether particularly simple TiO_2 nanotube sensors could be constructed based on nanotubes by ALD on nanocellulose templates and subsequent calcination. Measuring conductivity of a dropcast TiO_2 nanotube film reveals a dependence of resistance to the humidity of the environment. The humidity sensitivity of dropcast TiO_2 nanotube films was tested in air and argon atmosphere and the electrical response between two electrodes was reproducible. The response of resistance and capacitance to humidity is shown in Figure 4. From relative humidity of 0−40% there was barely any change in resistance, but going from 40 to 80% the resistance decreased to 1/30th of the original value. The response is linear on a logarithmic scale with respect to the relative humidity. A similar increase in capacitance over the same region was also observed. Both of these changes were reversible. After prolonged exposure to a dry atmosphere the samples had a higher resistance, but they returned to the reversible curve after being exposed to humidity.

In the TiO_2 nanotube films, some tubes form continuous paths from electrode to electrode while others are dead ends. We assume that the dead ends contribute to the capacitance of the film and the current flows through the continuous network. The change in resistance upon humidity can be tentatively explained simply by the water adsorbed on the surface of the tubes, which can increase the conductivity of the system. Because there is a high surface area on the tubes, the effect of surfaces and adsorption is pronounced compared to flat films. The change in capacitance could be addressed to change in the

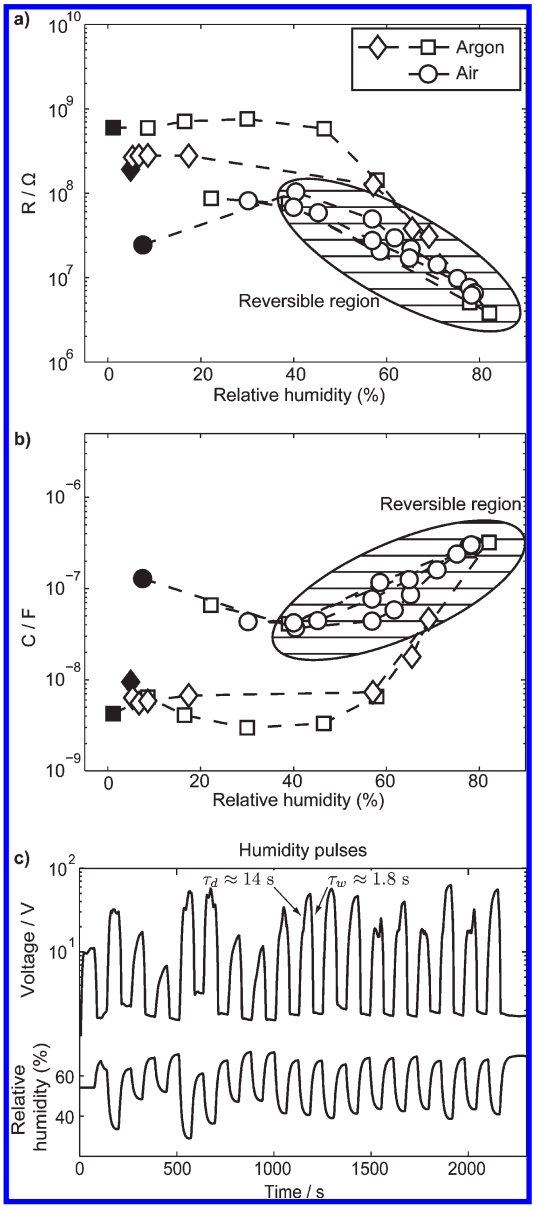

Figure 4. (a) Resistance and (b) capacitance of a dropcast TiO_2 nanotube film (four-point measurement) as a function of relative humidity measured in air and argon. The filled symbols mark the starts of the experiments. On logarithmic scale there is a linear, reversible response to humidity in region 40−80% after the initial exposure to water vapor. (c) The plot shows the time response of applied voltage (at fixed current, two-point measurement) to changes in atmosphere humidity. Response to humid air is fast with time constant, τ_w, less than 2 s. A running average has been taken over the voltage data to reduce measurement noise and increase readability of the plot.

dielectric constant, ε, of the insulating medium. Water has higher ε than any of the gases and the capacitance of a simple plate capacitor is of the form $C \propto \varepsilon$, therefore the capacitance would increase with increasing humidity, as observed. Figure 4 also shows that the voltage response of a TiO_2 nanotube film (at steady current) is correlated with the humidity of the chamber. We assume a simple exponential shape $U(t) \propto e^{-t/\tau}$ for the response with a time constant τ. The response to humidity was very rapid with a time constant

τ_w less than 2 s. Simply by breathing out humid air on top of the sample, a decrease in applied voltage is observed due to the local humidity increase. A reverse behavior was observed when a sample was blown with pressurized dry air. In this case τ_d was *ca.* 14 s.

There have been a few reports on neat TiO_2 films or nanostructures acting as humidity sensors.[53,54,56] Zhang *et al.* reported a resistive humidity sensor from a TiO_2 nanotube array, and it was tested with different calcination temperatures.[54] The calcination temperature affects the crystal form of TiO_2, and rutile form provided the best results for sensing. A sample calcinated at 600 °C gave the best response with response times of 100 and 190 s for dry (5%) and humid (95%) air. Our response times are 10−100 times faster than these values. Steele *et al.* made a rutile TiO_2 humidity sensor with subsecond response times,[56] but their sensor is capacitive and it is not based on nanowires or nanotubes. For comparison, the commercial Vaisala humidity meter we used as reference has a reported response time of *ca.* 8 s.

CONCLUSION

We have demonstrated a facile route for preparation of hollow inorganic nanotube aerogels based on ALD on native nanocellulose aerogel templates and removal of the template by calcination. Nanocellulose aerogels were prepared by freeze-drying and supercritical drying. Different drying methods were compared: liquid nitrogen freeze-drying leads to sheetlike aggregation, liquid propane freeze-drying enabled fibrillar structures up to sample thicknesses of ca. 2 mm, whereas supercritically dried aerogels showed no aggregation even in centimeter thick samples. The nanocellulose aerogels can readily be uniformly coated with different inorganic oxides (ZnO, TiO_2, and Al_2O_3) by atomic layer deposition. We demonstrate that the inorganic−organic aerogel can be calcinated to obtain a purely inorganic hollow nanotube aerogel. Porous films can be prepared by dispersing the inorganic nanotubes into a solvent and then casting it on a substrate. A TiO_2 nanotube humidity sensor with relatively fast response times in the humidity region of 40−80% was demonstrated.

Inorganic hollow nanotube aerogel networks could have future applications in functional materials, such as nonwetting surfaces, sensors, and carriers and also in encapsulation, drug-release, catalysis, microfluidic devices, and filtration.

MATERIALS AND METHODS

Materials. Nanocellulose hydrogel (never-dried hardwood kraft pulp) was kindly received from VTT/UPM. Preparation of the hydrogel is described elsewhere.[28] Fluorine tin oxide (FTO) covered glass with resistivity of 15 Ω/cm^2 was purchased from Solaronix SA. Substrates were cleaned by sonication in mild detergent, acetone, and ethanol and then dried with a stream of pressurized air.

Aerogel Preparation. An overview of the preparation process is shown in Figure 1. Nanocellulose aerogel samples were prepared using three different methods: freeze-drying using liquid nitrogen, freeze-drying using liquid propane, and supercritical CO_2 drying. For comparison, we also made a sample by ambient drying by placing nanocellulose hydrogel into a refrigerator (+4 °C, atmospheric pressure).

Freeze-Drying. An aqueous nanocellulose hydrogel with 1.7% solid content was applied to a metallic mold of 50 × 50 × 2 mm^3 dimensions. The films were made thin (2 mm) to shorten the time required to freeze the whole sample. The mold filled with hydrogel was then plunged into either cooled liquid propane (*ca.* −100 °C) or liquid nitrogen (−196 °C). Molds were then placed onto a cooled metal block, which serves as a cold reservoir to prevent melting, and then quickly transferred into a vacuum chamber where sublimation of the ice took place resulting in a porous aerogel structure.

Supercritical CO_2 Drying. The first step in the process is to exchange the solvent to acetone, which mixes well with water and CO_2. Cellulose hydrogel was placed in a beaker and covered with acetone. The acetone was changed at least twice a day over 3 days. The gel was centrifuged and the top layer of solvent was gently removed. The gel was then diluted with acetone and the process was repeated. A Baltec CPD 030 device was used for the supercritical drying. First the acetone filled chamber is cooled below the liquidification point of CO_2, and then the chamber is cyclically filled with CO_2 and then emptied, while keeping the sample immersed in CO_2. The process was repeated at least seven times with 5−15 min between the steps. Last the chamber was heated to 40 °C, and CO_2 went beyond the critical point. The pressure was then slowly released while maintaining the temperature at 40 °C.

Atomic Layer Deposition. ALD was performed in a commercial ASM Microchemistry Ltd. F-120 flow-type reactor. Nitrogen (>99.999%) generated by a Schmidlin UHPN 3000 N_2 generator was used as carrier gas as well as for purging between precursor pulses. Diethyl zinc (DEZ) was acquired from Crompton GmbH. Trimethyl aluminum (TMA) was used as aluminum precursor (Witco GmbH, purity 99%). Titanium tetrachloride ($TiCl_4$) was used to deposit titanium dioxide (Sigma-Aldrich, purity 99%). Distilled water was used as the oxygen source in all cases. Basic ALD processes for ZnO and Al_2O_3 follow the well-established routes for metalorganics (DEZ/H_2O and TMA/H_2O), and the TiO_2 process follows the route for halides ($TiCl_4$/H_2O).[42] ALD was done at a relatively low temperature of 150 °C to prevent decomposition of cellulose. To achieve conformal coatings on the aerogels, we employed pulse and purge times in excess of 20 s to allow adequate diffusion times for the precursors to infiltrate into the porous substrates.

It is difficult to get rid of the adsorbed water on the nanocellulose aerogels.[40] Therefore we first heated the samples to 150 °C and kept them in a 1−3 mbar pressure for at least 1 h prior to deposition. First a long pulse of the inorganic precursor was released into the chamber, and the sample was exposed for 30 min to allow the precursor to react with the residual water. Then the chamber was thoroughly purged, and we assumed that all of the excess water reacted and an initial layer of oxide formed on the aerogel fibrils. After the initial deposition cycle, the ALD-type sequential deposition was performed. It consisted of 20−30 s long pulses followed by 30−60 s purging with nitrogen. The thickness of the resulting layers is controlled by the number of deposition cycles. Usually 50 ALD cycles were deposited, but also up to 300 cycles were tested.

TiO_2 Nanotube Films. A fibrillar aerogel coated with 50 ALD cycles of TiO_2 was first calcinated at 450 °C for 8 h to decompose the cellulose and to get empty inorganic tube networks. Then the inorganic aerogel was crushed in a mortar, dispersed in ethanol (*ca.* 2% w/w), and sonicated in a bath. A 5 × 8 mm^2 film was cast on a glass substrate masked with Scotch tape. The mask was removed and the film was let to dry on a hot plate set at 60 °C. Then the film was placed in a 450 °C oven for 30 min.

Characterization Techniques. Field-emission scanning electron microscopy (JEOL JSM-7500FA) was performed at 5 keV electron energy or below. The neat aerogels were sputtered with a thin layer of platinum (Emitech K950X/K350) to promote conductivity. JSM-7500FA is equipped with a JEOL energy-dispersive X-ray analysis addition with a Be thin film window and liquid nitrogen cooled detector. A spot spectrum was taken over 2 min using 15 keV electron energy to analyze the composition of samples. Quantitative analysis was done by comparing the area of the fitted K_α or L_α peaks.

Transmission electron microscopy (TEM) was performed on a FEI Tecnai 12 operating at 120 kV. Dry samples were ground with a mortar and then applied on a carbon film support grid. Imaging was done in bright-field mode with slight underfocus.

Conductivity Measurements. The conductivity of TiO_2 nanotube films was measured with a four-point setup, consisting of a Keithley 2400 sourcemeter connected to a TestPoint measurement program. To ensure that the substrate did not contribute to the results, samples were made on two different substrates: evaporated gold (four-point measurement) electrodes and FTO glass divided in half (two-point measurement). Spacing of gold electrodes was 1 mm and it was less (*ca.* 0.5 mm) for the scratch on the FTO glass. A current profile (0; I_{max}; $-I_{max}$; $I_{max}/2$; $-I_{max}/2$; 0) was run, and the voltage across the measurement probes was recorded. To extract resistance and capacitance values, the sample was modeled as a parallel RC-circuit with Matlab and Simulink. Fitting was done using the least-squares method, and since only qualitative data was needed, the result was estimated by visually comparing the fitted result to the data. Fits were of good quality at relative humidities over *ca.* 40%.

Humidity in the measurement chamber was controlled by flowing a gas (air or argon) through a bubbler with deionized water and then mixing it with dry gas. Humidity and temperature were recorded with a Vaisala HMT333 logging temperature/humidity transmitter. Measurements were done in stable room temperature (22−24 °C), and the humidity was let to stabilize at least 15 min between measurements. Before the experiments, the samples were kept overnight in a dark, dry atmosphere to exclude the effect of photoinduced wetting.[57] Samples were also kept in the dark during the course of the humidity sensing experiment. To test the time dependence of the response, humid air was streamed straight onto the sample. The current flowing through the sample was fixed, and the voltage across terminals was recorded. Speed of response was estimated by fitting an exponential decay function to the data.

Acknowledgment. Funding from the Academy of Finland and from the NASEVA project funded by the Finnish Funding Agency for Technology and Innovation (TEKES) are acknowledged. This work made use of the facilities of Nanomicroscopy Center at Aalto University (Aalto-NMC).

Supporting Information Available: Inorganic layer thickness data (S1), larger SEM micrographs of single nanocellulose fibrils (S2), several samples demonstrating differences in preparation methods (S3, S4) and different coatings (S5−S7), XRD data for a TiO_2 nanotube film (S8). This material is available free of charge *via* the Internet at http://pubs.acs.org.

REFERENCES AND NOTES

1. Xia, Y.; Yang, P.; Sun, Y.; Wu, Y.; Mayers, B.; Gates, B.; Yin, Y.; Kim, F.; Yan, H. One-Dimensional Nanostructures: Synthesis, Characterization, and Applications. *Adv. Mater.* **2003,** *15*, 353–389.
2. Lieber, C. M.; Wang, Z. L. Functional Nanowires. *Mater. Res. Bull.* **2007,** *32*, 99–108.
3. Remškar, M. Inorganic Nanotubes. *Adv. Mater.* **2004,** *16*, 1497–1504.
4. Imai, H.; Takei, Y.; Shimizu, K.; Matsuda, M.; Hirashima, H. Direct Preparation of Anatase TiO_2 Nanotubes in Porous Alumina Membranes. *J. Mater. Chem.* **1999,** *9*, 2971–2972.
5. Lee, S. B.; Mitchell, D. T.; Trofin, L.; Nevanen, T. K.; Soderlund, H.; Martin, C. R. Antibody-Based Bio-Nanotube Membranes for Enantiomeric Drug Separations. *Science* **2002,** *296*, 2198–2200.
6. Daub, M.; Knez, M.; Goesele, U.; Nielsch, K. Ferromagnetic Nanotubes by Atomic Layer Deposition in Anodic Alumina Membranes. *J. Appl. Phys.* **2007,** *101*, 09J111.
7. Foong, T. R. B.; Shen, Y.; Hu, X.; Sellinger, A. Template-Directed Liquid ALD Growth of TiO_2 Nanotube Arrays: Properties and Potential in Photovoltaic Devices. *Adv. Funct. Mater.* **2010,** *20*, 1390–1396.
8. Wang, J.; Cui, Y.; Li, H.; Wang, Z.; Huang, K.; Sun, G. *In Situ* Synthesis and Characterization of TiO_2 Nanoarray Films. *Res. Chem. Intermed.* **2010,** *36*, 17–26.
9. Varghese, O. K.; Paulose, M.; Grimes, C. A. Long Vertically Aligned Titania Nanotubes on Transparent Conducting Oxide for Highly Efficient Solar Cells. *Nature Nanotech.* **2009,** *4*, 592–597.
10. Ras, R. H. A.; Ruotsalainen, T.; Laurikainen, K.; Linder, M. B.; Ikkala, O. Hollow Nanoparticle Nanotubes with a Nanoscale Brick Wall Structure of Clay Mineral Platelets. *Chem. Commun.* **2007,** 1366–1368.
11. Kim, G. M.; Lee, S. M.; Michler, G. H.; Roggendorf, H.; Gösele, U.; Knez, M. Nanostructured Pure Anatase Titania Tubes Replicated from Electrospun Polymer Fiber Templates by Atomic Layer Deposition. *Chem. Mater.* **2008,** *20*, 3085–3091.
12. Ras, R. H. A.; Kemell, M.; de Wit, J.; Ritala, M.; ten Brinke, G.; Leskelä, M.; Ikkala, O. Hollow Inorganic Nanospheres and Nanotubes with Tunable Wall Thicknesses by Atomic Layer Deposition on Self-Assembled Polymeric Templates. *Adv. Mater.* **2007,** *19*, 102–106.
13. Kistler, S. S. Coherent Expanded Aerogels and Jellies. *Nature* **1931,** *127*, 741–741.
14. Aerogel. The History of Aerogel. http://www.aerogel.org/?cat=38 (accessed Feb 14, 2011).
15. Hüsing, N.; Schubert, U. Aerogels—Airy Materials: Chemistry, Structure, and Properties. *Angew. Chem., Int. Ed.* **1998,** *37*, 22–45.
16. Pierre, A. C.; Pajonk, G. M. Chemistry of Aerogels and Their Applications. *Chem. Rev.* **2002,** *102*, 4243–4266.
17. Kim, D. Y.; Nishiyama, Y.; Wada, M.; Kuga, S. Graphitization of Highly Crystalline Cellulose. *Carbon* **2001,** *39*, 1051–1056.
18. Ishida, O.; Kim, D. Y.; Kuga, S.; Nishiyama, Y.; Brown, R. M. Microfibrillar Carbon from Native Cellulose. *Cellulose* **2004,** *11*, 475–480.
19. Kuga, S.; Kim, D. Y.; Nishiyama, Y.; Brown, R. M. Nanofibrillar Carbon from Native Cellulose. *Mol. Cryst. Liq. Cryst.* **2002,** *387*, 237–243.
20. Luong, N. D.; Lee, Y.; Nam, J. D. Facile Transformation of Nanofibrillar Polymer Aerogel to Carbon Nanorods Catalyzed by Platinum Nanoparticles. *J. Mater. Chem.* **2008,** *18*, 4254–4259.
21. Grzyb, B.; Hildenbrand, C.; Berthon-Fabry, S.; Begin, D.; Job, N.; Rigacci, A.; Achard, P. Functionalisation and Chemical Characterisation of Cellulose-Derived Carbon Aerogels. *Carbon* **2010,** *48*, 2297–2307.
22. Poco, J. F.; Satcher, J. H.; Hrubesh, L. W. Synthesis of High Porosity, Monolithic Alumina Aerogels. *J. Non-Cryst. Solids* **2001,** *285*, 57–63.
23. Gao, Y. P.; Sisk, C. N.; Hope-Weeks, L. J. A Sol−Gel Route to Synthesize Monolithic Zinc Oxide Aerogels. *Chem. Mater.* **2007,** *19*, 6007–6011.
24. Eichhorn, S. J.; Dufresne, A.; Aranguren, M.; Marcovich, N. E.; Capadona, J. R.; Rowan, S. J.; Weder, C.; Thielemans, W.; Roman, M.; Renneckar, S.; *et al.* Review: Current International Research into Cellulose Nanofibres and Nanocomposites. *J. Mater. Sci.* **2010,** *45*, 1–33.
25. Turbak, A. F.; Snyder, F. W.; Sandberg, K. R. Microfibrillated Cellulose, a New Cellulose Product: Properties, Uses and Commercial Potential. *J. Appl. Polym. Sci.: Appl. Polym. Symp.* **1983,** *37*, 815–827.
26. Abe, K.; Iwamoto, S.; Yano, H. Obtaining Cellulose Nanofibers with a Uniform Width of 15 nm from Wood. *Biomacromolecules* **2007,** *8*, 3276–3278.
27. Saito, T.; Kimura, S.; Nishiyama, Y.; Isogai, A. Cellulose Nanofibers Prepared by TEMPO-Mediated Oxidation of Native Cellulose. *Biomacromolecules* **2007,** *8*, 2485–2491.

28. Pääkkö, M.; Ankerfors, M.; Kosonen, H.; Nykänen, A.; Ahola, S.; Österberg, M.; Ruokolainen, J.; Laine, J.; Larsson, P. T.; Ikkala, O.; *et al.*Enzymatic Hydrolysis Combined with Mechanical Shearing and High-Pressure Homogenization for Nanoscale Cellulose Fibrils and Strong Gels. *Biomacromolecules* **2007,** *8*, 1934–1941.
29. Henriksson, M.; Henriksson, G.; Berglund, L. A.; Lindstrom, T. An Environmentally Friendly Method for Enzyme-Assisted Preparation of Microfibrillated Cellulose (MFC) Nanofibers. *Eur. Polym. J.* **2007,** *43*, 3434–3441.
30. Tan, C.; Fung, B. M.; Newman, J. K.; Vu, C. Organic Aerogels with Very High Impact Strength. *Adv. Mater.* **2001,** *13*, 644–646.
31. Jin, H.; Nishiyama, Y.; Wada, M.; Kuga, S. Nanofibrillar Cellulose Aerogels. *Colloids Surf., A* **2004,** *240*, 63–67.
32. Gavillon, R.; Budtova, T. Aerocellulose: New Highly Porous Cellulose Prepared from Cellulose-NaOH Aqueous Solutions. *Biomacromolecules* **2008,** *9*, 269–277.
33. Pääkkö, M.; Vapaavuori, J.; Silvennoinen, R.; Kosonen, H.; Ankerfors, M.; Lindström, T.; Berglund, L. A.; Ikkala, O. Long and Entangled Native Cellulose I Nanofibers Allow Flexible Aerogels and Hierarchically Porous Templates for Functionalities. *Soft Matter* **2008,** *4*, 2492–2499.
34. Olsson, R. T.; Azizi Samir, M. A. S.; Salazar Alvarez, G.; Belova, L.; Strom, V.; Berglund, L. A.; Ikkala, O.; Nogues, J.; Gedde, U. W. Making Flexible Magnetic Aerogels and Stiff Magnetic Nanopaper Using Cellulose Nanofibrils as Templates. *Nature Nanotech.* **2010,** *5*, 584–588.
35. Svagan, A. J.; Samir, M. A. S. A.; Berglund, L. A. Biomimetic Foams of High Mechanical Performance Based on Nanostructured Cell Walls Reinforced by Native Cellulose Nanofibrils. *Adv. Mater.* **2008,** *20*, 1263–1269.
36. Sehaqui, H.; Salajkova, M.; Zhou, Q.; Berglund, L. A. Mechanical Performance Tailoring of Tough Ultra-High Porosity Foams Prepared from Cellulose I Nanofiber Suspensions. *Soft Matter* **2010,** *6*, 1824–1832.
37. Duchemin, B. J. C.; Staiger, M. P.; Tucker, N.; Newman, R. H. Aerocellulose Based on All-Cellulose Composites. *J. Appl. Polym. Sci.* **2010,** *115*, 216–221.
38. Liebner, F.; Haimer, E.; Wendland, M.; Neouze, M. A.; Schlufter, K.; Miethe, P.; Heinze, T.; Potthast, A.; Rosenau, T. Aerogels from Unaltered Bacterial Cellulose: Application of $scCO_2$ Drying for the Preparation of Shaped, Ultra-Lightweight Cellulosic Aerogels. *Macromol. Biosci.* **2010,** *10*, 349–352.
39. Ikkala, O.; Ras, R. H. A.; Houbenov, N.; Ruokolainen, J.; Pääkkö, M.; Laine, J.; Leskelä, M.; Berglund, L. A.; Lindström, T.; ten Brinke, G.; *et al.* Solid State Nanofibers Based on Self-Assemblies: from Cleaving from Self-Assemblies to Multilevel Hierarchical Constructs. *Faraday Discuss.* **2009,** *143*, 95–107.
40. Kettunen, M.; Silvennoinen, R. J.; Houbenov, N.; Nykänen, A.; Ruokolainen, J.; Sainio, J.; Pore, V.; Kemell, M.; Ankerfors, M.; Lindström, T.; *et al.* Photoswitchable Superabsorbency Based on Nanocellulose Aerogels. *Adv. Funct. Mater.* **2011,** *21*, 510–517.
41. Leskelä, M.; Ritala, M. Atomic Layer Deposition Chemistry: Recent Developments and Future Challenges. *Angew. Chem., Int. Ed.* **2003,** *42*, 5548–5554.
42. Puurunen, R. L. Surface Chemistry of Atomic Layer Deposition: A Case Study for the Trimethylaluminum/Water Process. *J. Appl. Phys.* **2005,** *97*, 121301/1–52.
43. Knez, M.; Nielsch, K.; Niinistö, L. Synthesis and Surface Engineering of Complex Nanostructures by Atomic Layer Deposition. *Adv. Mater.* **2007,** *19*, 3425–3438.
44. George, S. M. Atomic Layer Deposition: An Overview. *Chem. Rev.* **2009,** *110*, 111–131.
45. Shin, H.; Jeong, D. K.; Lee, J.; Sung, M.; Kim, J. Formation of TiO_2 and ZrO_2 Nanotubes Using Atomic Layer Deposition with Ultraprecise Control of the Wall Thickness. *Adv. Mater.* **2004,** *16*, 1197–1200.
46. Kemell, M.; Pore, V.; Ritala, M.; Leskelä, M.; Lindén, M. Atomic Layer Deposition in Nanometer-Level Replication of Cellulosic Substances and Preparation of Photocatalytic TiO_2/Cellulose Composites. *J. Am. Chem. Soc.* **2005,** *127*, 14178–14179.
47. Triani, G.; Evans, P. J.; Attard, D. J.; Prince, K. E.; Bartlett, J.; Tan, S.; Burford, R. P. Nanostructured TiO_2 Membranes by Atomic Layer Deposition. *J. Mater. Chem.* **2006,** *16*, 1355–1359.
48. Hyde, G. K.; Park, K. J.; Stewart, S. M.; Hinestroza, J. P.; Parsons, G. N. Atomic Layer Deposition of Conformal Inorganic Nanoscale Coatings on Three-Dimensional Natural Fiber Systems: Effect of Surface Topology on Film Growth Characteristics. *Langmuir* **2007,** *23*, 9844–9849.
49. Hamann, T. W.; Martinson, A. B. E.; Elam, J. W.; Pellin, M. J.; Hupp, J. T. Aerogel Templated ZnO Dye-Sensitized Solar Cells. *Adv. Mater.* **2008,** *20*, 1560–1564.
50. Hamann, T. W.; Martinson, A. B. F.; Elam, J. W.; Pellin, M. J.; Hupp, J. T. Atomic Layer Deposition of TiO_2 on Aerogel Templates: New Photoanodes for Dye-Sensitized Solar Cells. *J. Phys. Chem. C* **2008,** *112*, 10303–10307.
51. Crossland, E. J. W.; Kamperman, M.; Nedelcu, M.; Ducati, C.; Wiesner, U.; Smilgies, D. M.; Toombes, G. E. S.; Hillmyer, M. A.; Ludwigs, S.; Steiner, U.; *et al.* A Bicontinuous Double Gyroid Hybrid Solar Cell. *Nano Lett.* **2009,** *9*, 2807–2812.
52. Leidenfrost, J. G. On Fixation of Water in Diverse Fire. *Int. J. Heat Mass Transfer* **1966,** *9*, 1153–1166.
53. Yang, L.; Luo, S.; Cai, Q.; Yao, S. A Review on TiO_2 Nanotube Arrays: Fabrication, Properties, and Sensing Applications. *Chin. Sci. Bull.* **2010,** *55*, 331–338.
54. Zhang, Y.; Fu, W.; Yang, H.; Qi, Q.; Zeng, Y.; Zhang, T.; Ge, R.; Zou, G. Synthesis and Characterization of TiO_2 Nanotubes for Humidity Sensing. *Appl. Surf. Sci.* **2008,** *254*, 5545–5547.
55. Ramgir, N. S.; Yang, Y.; Zacharias, M. Nanowire-Based Sensors. *Small* **2010,** *6*, 1705–1722.
56. Steele, J. J.; Taschuk, M. T.; Brett, M. J. Response Time of Nanostructured Relative Humidity Sensors. *Sens. Actuators, B* **2009,** *140*, 610–615.
57. Malm, J.; Sahramo, E.; Karppinen, M.; Ras, R. H. A. Photo-Controlled Wettability Switching by Conformal Coating of Nanoscale Topographies with Ultrathin Oxide Films. *Chem. Mater.* **2010,** *22*, 3349–3352.